Large-scale simulations of snow albedo masking by forests

Large-scale simulations of snow albedo masking by forests

Richard Essery[1]

[1] Comparisons between climate models have found large differences in predictions for the albedo of forested regions with snow cover, leading to uncertainty in the strength of snow albedo feedbacks on climate change predicted by these models. To explore this uncertainty, three commonly used methods for calculating the albedo of vegetated surfaces are compared, taking observed snow and vegetation distributions as inputs. Surprisingly, all three methods produce similar results and compare reasonably well with observations over seasonally snow-covered regions of the Northern Hemisphere. It appears that some climate models use unrealistic parameter values, and snow albedo masking need not be as large a source of uncertainty as it is in current climate projections. **Citation:** Essery, R. (2013), Large-scale simulations of snow albedo masking by forests, *Geophys. Res. Lett.*, *40*, doi:10.1002/grl.51008.

1. Introduction

[2] Fresh, deep snow has a high albedo, but densely forested landscapes retain low albedos when there is snow on the ground, even with significant amounts of snow held in the canopy. The existence of boreal forests is thought to have a warming effect on climate because of this snow albedo masking effect [*Bonan et al.*, 1992; *Brovkin et al.*, 2009], which needs to be accurately represented in climate models. Unfortunately, *Roesch* [2006] found large winter and spring albedo biases over forested regions in the Third Coupled Model Intercomparison Project (CMIP3) climate simulations submitted for the Intergovernmental Panel on Climate Change (IPCC) Fourth IPCC Assessment Report (AR4) [*Randall et al.*, 2007]. Land surface parametrizations in several of the participating models have been updated since AR4, so it might be thought that the model biases would have been reduced. On the contrary, this problem has gained renewed urgency in the run up to the publication of AR5 with the discovery by *Qu and Hall* [2013] that a large snow albedo spread persists in simulations submitted for CMIP5. Moreover, the resulting spread in snow albedo feedback strength accounts for much of the spread in model predictions of warming over Northern Hemisphere land. *Qu and Hall* [2013] concluded that using observations to constrain modeled albedos of heavily vegetated landscapes with snow cover would reduce uncertainty in predictions of regional climate change for physically consistent reasons.

[3] A dark band crossing the continents of the Northern Hemisphere can be clearly identified in maps of maximum albedo for seasonally snow-covered land that were obtained from Defense Meteorological Satellite Program data by *Robinson and Kukla* [1985] and from Moderate Resolution Imaging Spectroradiometer (MODIS) data by *Barlage et al.* [2005]. The same feature can be seen in Figure 1a, which shows average snow-covered albedos (calculated by averaging broadband white-sky albedos for every 16 day period flagged as having 100% snow cover in each 0.05° pixel of the MODIS MCD43C3 Collection 5 product [*Schaaf et al.*, 2002] between 1 January 2006 and 27 December 2010). The pattern of areas with low snow-covered albedo has strong similarities with the maps of forest fraction in Figure 2, which will be discussed in more detail later.

[4] In this letter, three common methods for calculating the albedo of snow-covered forests in climate models are compared with large-scale observations. Spatial patterns and seasonal cycles of albedo are considered. Rather than taking results from climate models, albedo parametrizations are run in isolation with snow cover, snowfall, and temperature inputs.

2. Snow Albedo Masking in Climate Models

[5] *Qu and Hall* [2007] classified CMIP3 models into four types according to how they calculate surface albedo depending on snow and vegetation cover. The simplest models have albedos that depend on snow depth but are independent of vegetation cover; it has long been known that this approach is unrealistic [*Thomas and Rowntree*, 1992; *Viterbo and Betts*, 1999], and it is not discussed further here. The next simplest approach (Qu and Hall type 3) is to calculate albedo α as a weighted average

$$\alpha = (1 - f_s)\alpha_0 + f_s\alpha_s \qquad (1)$$

where α_0 and α_s are snow-free and deep-snow albedos, both of which depend on vegetation type, and f_s is the fraction of the surface covered by snow. Effective values may be specified for each model grid cell, or the albedos of different surface types within a cell may be weighted by their fractional coverages. An example of this type of model is the MOSES land surface scheme [*Cox et al.*, 1999] used in the Hadley Centre Coupled Model, in which deep-snow albedos for open and forested surfaces are based on airborne measurements by *Robinson and Kukla* [1984].

[6] The most common type of model in CMIP3 according to Qu and Hall (type 2) distinguishes between snow intercepted in forest canopies and snow on the ground, as in the European Centre for Medium-Range Weather Forecasts (ECMWF) Hamburg 5 (ECHAM5) climate model [*Roesch and Roeckner*, 2006]. The albedo is

$$\alpha = f_g\left[(1 - f_s)\alpha_{g0} + f_s\alpha_{gs}\right] + (1 - f_g)\left[(1 - f_c)\alpha_{c0} + f_c\alpha_{cs}\right] \qquad (2)$$
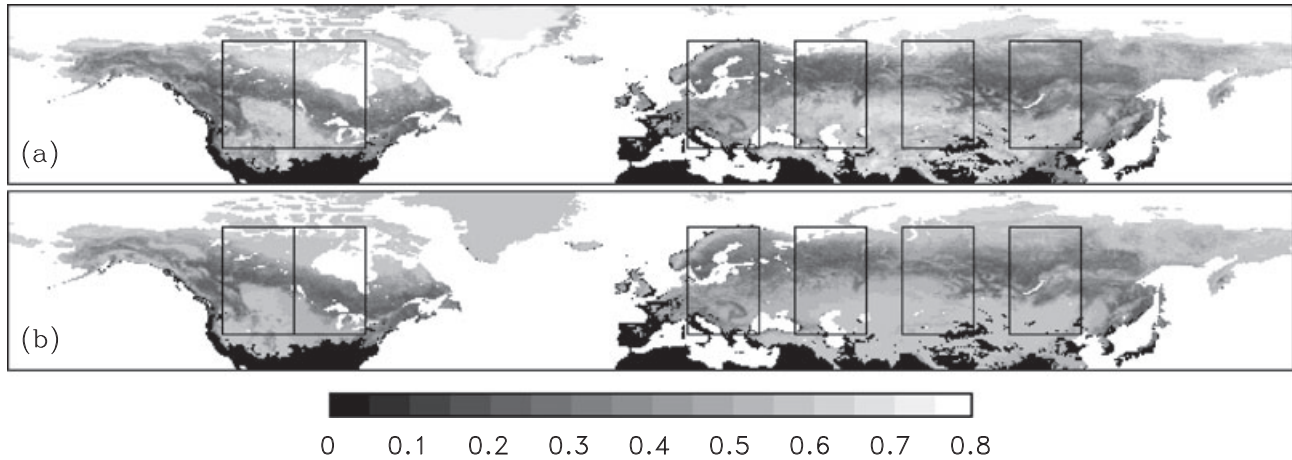
Figure 1. Average albedos for land with snow cover from (a) MODIS and (b) equation (1). Black pixels have missing data or no observed snow cover for 2006–2010. Boxes identify areas for which averages are presented in Figure 3.

where f_g is the canopy gap fraction, α_{gs} and α_{g0} are the albedos of snow on the ground and snow-free ground, f_c is the snow-covered fraction of the canopy with albedo α_{cs}, and α_{c0} is the albedo of the snow-free canopy. ECHAM5 sets $\alpha_{cs} = 0.2$ and calculates the gap fraction as $f_g = \exp(-\Lambda)$ for forests with plant area index Λ (including leaves and stems). A single albedo is calculated for all angles and wavelengths of illumination, but the Canadian Land Surface Scheme (CLASS) [*Verseghy et al.*, 1993; *Bartlett et al.*, 2006] in the Canadian Global Climate Model uses a similar approach to calculate separate albedos for direct beam and diffuse radiation in visible and near-infrared wavebands.

[7] The most sophisticated albedo calculations (Qu and Hall type 1) use canopy radiative transfer models. Although highly detailed models have been developed [*Widlowski et al.*, 2007], climate models use simpler two-stream approximations for canopy radiative transfer [*Dickinson*, 1983]. An example of this type of model is the CLM land surface scheme [*Oleson et al.*, 2010] used in the Community Climate System Model. Despite their relative simplicity, the two-stream albedo calculations are much too long to reproduce

here; they are fully described in the CLM documentation [*Oleson et al.*, 2010], and the subset of calculations used here is described in the supporting information. In addition to leaf and stem area indices, spectral reflectance and transmittance properties are required for canopy elements with and without snow cover. These parameters are fixed for each vegetation type in CLM, but *Pinty et al.* [2004] discussed how effective parameter value maps might be retrieved from remote sensing. For dense needleleaf forests which completely mask the albedo of the underlying ground, CLM parameter values give a snow-free albedo of 0.1 and a maximum albedo of 0.25 with snow on the canopy.

3. Methodology and Results

[8] Maps of vegetation distributions for use in climate models have been obtained from atlases [e.g., *Wilson and Henderson-Sellers*, 1985], remote sensing [e.g., *Hansen et al.*, 2000], and dynamic vegetation models [e.g., *Bonan et al.*, 2003]. Surface products from remote sensing are provided on grids or divided by biome classifications such as
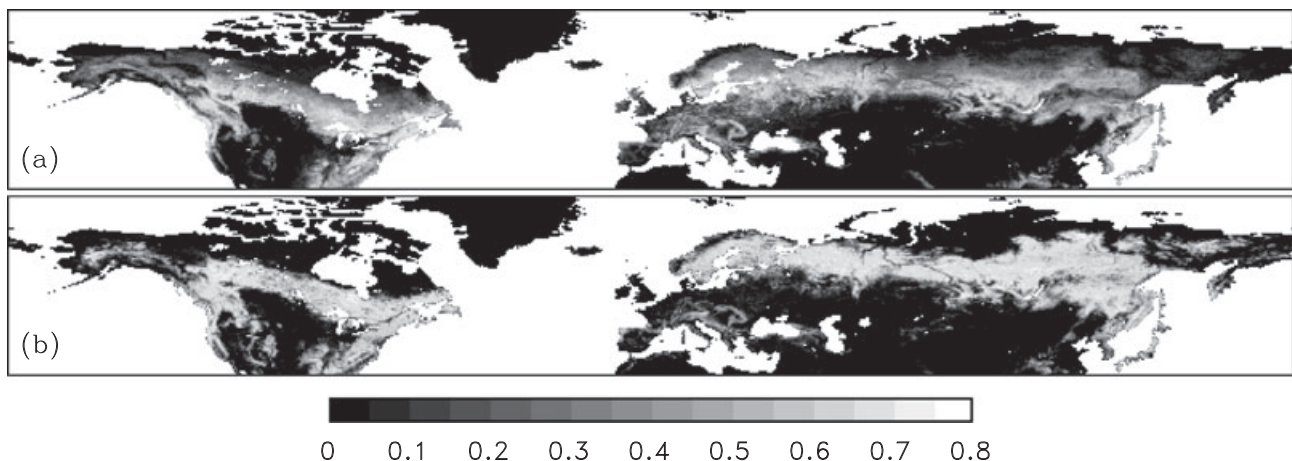

Figure 2. Forest fractions derived from (a) MODIS data for the Community Land Model (CLM) and (b) Advanced Very High Resolution Radiometer (AVHRR) data for the Met Office Surface Exchange Scheme (MOSES).

Table 1. Snow-Free and Snow-Covered PFT Albedos Obtained by Fitting Equation (1) With AVHRR or MODIS Land Cover Maps to MODIS Albedo Maps

	AVHRR		MODIS	
PFT	α_0	α_s	α_0	α_s
Broadleaf tree	0.13[a]	0.23[a]	0.16[b]	0.17[a]
Needleleaf tree	0.08[a]	0.17[a]	0.06[b]	0.06[a]
Grass	0.18[a]	0.52[a]	0.17[c]	0.55[c]
Shrub	0.14[a]	0.50[a]	0.13[c]	0.62[c]

[a] Used in simulations with equation (1) only.
[b] Used in simulations with equations (1) and (2) only.
[c] Used in all simulations.

the International Geosphere-Biosphere Programme (IGBP) [*Loveland et al.*, 2000], but climate models now often use plant functional types onto which parameters have to be mapped [*Bonan et al.*, 2002]. For example, AVHRR land cover data [*Hansen et al.*, 2000] have been mapped from the 17 IGBP classes to fractions of five Plant Functional Types (PFTs) and four nonvegetated surface types for use in MOSES [*Essery et al.*, 2003]. *Lawrence and Chase* [2007] developed maps of PFT fractions and plant area indices consistent with MODIS surface products for use in CLM. The AVHRR/MOSES and MODIS/CLM maps of forest fraction shown in Figure 2 are similar, but close inspection reveals differences.

[9] Albedo parameters for needleleaf tree, broadleaf tree, grass, and shrub PFTs were obtained by fitting equation (1) to MODIS albedo maps with and without snow cover. Mean squared differences between predicted and observed albedos were minimized using Powell's method, giving the α_0 and α_s values in Table 1. Snow-free albedos obtained using either MODIS or AVHRR land cover are similar to each other and similar to those found by *Houldcroft et al.* [2009]. With snow, the MODIS land cover gives somewhat lower tree albedos and higher shrub albedos than AVHRR. These are not directly comparable with snow-covered MODIS albedos quoted for IGBP classes by *Barlage et al.* [2005], *Moody et al.* [2007], and *Flanner et al.* [2011].

3.1. Snow-Covered Albedo Simulations

[10] The three albedo masking parametrizations described above were run on a 0.5° Northern Hemisphere grid with snow completely covering the ground but no snow in the canopy ($f_s = 1$, $f_c = 0$). To focus on differences between forest albedo parametrizations, equation (1) was used for the albedo of grass, shrub, and open grid cell fractions in all three cases. Visible and near-infrared diffuse forest albedos from the two-stream approximation were averaged for comparison with the MODIS broadband white-sky albedo; the other parametrizations do not make these distinctions. March values of leaf and stem area indices from *Lawrence and Chase* [2007] were used in equation (2) and the two-stream approximation, giving area-average plant area indices of 3.1 for needleleaf trees and 0.8 for deciduous broadleaf trees.

[11] Figure 1b shows a snow-covered albedo map predicted by equation (1) with optimized parameters from Table 1 and MODIS land cover; the other two parametrizations produce very similar patterns dominated by the distribution of forests. Error statistics are given in Table 2, and zonal average albedos in 20° × 30° boxes are shown in

Figure 3 for all three parametrizations. Fitting equation (1) gives albedos that follow the observations closely, with low errors and high correlation; the largest errors occur above 60°N in the 80–100°W and 100–120°E boxes, which have extensive shrub cover and deciduous needleleaf forests, respectively. Equation (2) and the two-stream approximation give similar results but slightly higher errors without the benefit of fitting. Assuming complete canopy snow cover (f_c=1) increases positive biases in albedo because the snow-covered canopy albedo parameters taken from literature are higher than the optimized value for needleleaf trees.

[12] Fitting equation (1) to MODIS albedos using AVHRR land cover does not give quite as close a fit as using MODIS land cover (Table 2, Figure 3). There are notable differences between 50 and 60°N in the 10–30°E box, where the AVHRR land cover has lower forest fractions, and above 60°N in the 100–120°E box, where it has greater fractions.

3.2. Seasonal Albedo Cycle Simulations

[13] Climate models differ in how they parametrize the fractions of ground and canopy that are covered with snow for given masses of lying and intercepted snow, and there is little data for evaluation of these parametrizations on climate model grid scales. Here daily estimates of snow-covered fraction for 2006–2010 were obtained by averaging the Interactive Multisensor Snow and Ice Mapping System (IMS) 24 km binary snow cover analyses [*Helfrich et al.*, 2007] over 0.5° cells. Rather than trying to simulate the complex processes of snow interception, sublimation, melt, and unloading in canopies, a very simple parametrization based on CLASS and ECHAM5 is used. The rate of change in intercepted snow mass S_c for snowfall rate S_f is

$$\frac{dS_c}{dt} = cS_f - \tau^{-1}S_c \qquad (3)$$

with interception efficiency $c = 0.25$ and snow removal timescale $\tau = 10$ days. The intercepted load is limited to a maximum of $S_{c,\max} = 0.2\Lambda$, and all snows are removed from the canopy when the air temperature exceeds 0°C. The canopy snow cover fraction is simply set to $f_c = S_c/S_{c,\max}$. For decreasing snow albedo with age and increasing albedo with fresh snowfall, parametrizations from CLASS are used. The canopy interception and snow albedo parametrizations are driven with 6-hourly snowfall forecasts and air temperature analyses from ECMWF Re-Analysis-Interim [*Dee et al.*, 2011]. A MODIS-derived map of snow-free albedos from *Houldcroft et al.* [2009] is used for bare ground.

[14] Figure 4a shows observed and simulated seasonal cycles of albedo averaged over all land points between 40 and 70°N with valid MODIS data in 2006–2010. Because

Table 2. Biases, Root-Mean-Square (RMS) Errors and Correlations Between Snow-Covered Albedos Observed by MODIS and Predicted With Equation (1), Equation (2), or the Two-Stream Approximation

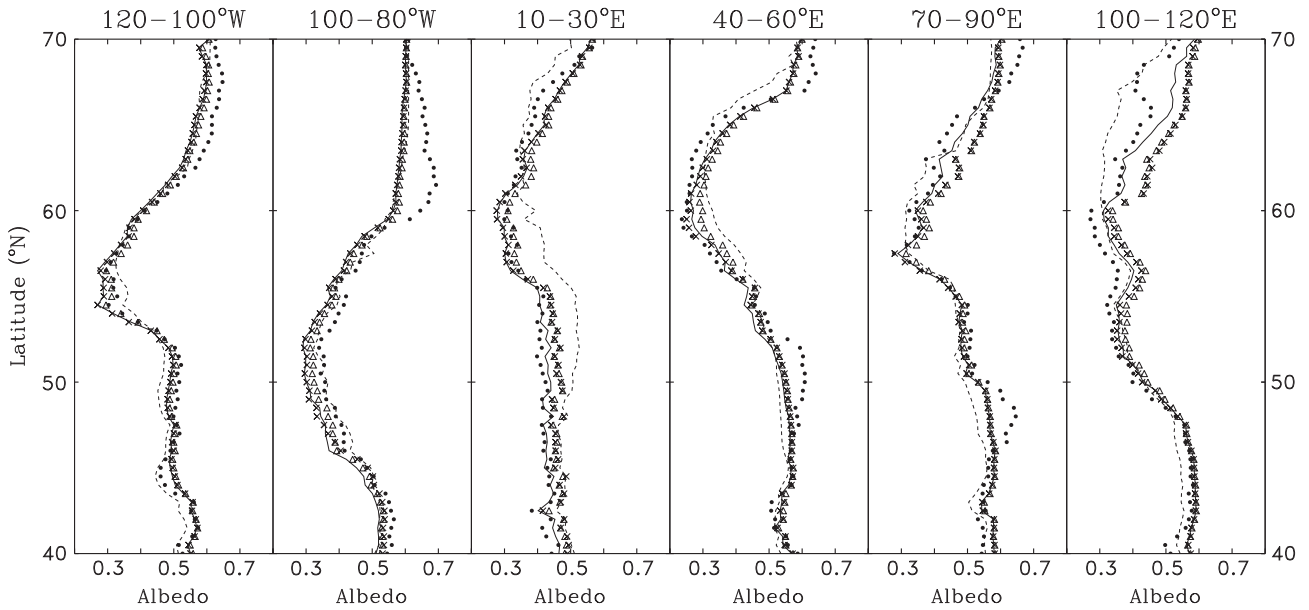|	Bias	RMS	Correlation
Equation (1) MODIS	0.004	0.05	0.92
Equation (1) AVHRR	0.01	0.09	0.75
Equation (2) $f_c = 0$	0.02	0.07	0.88
Equation (2) $f_c = 1$	0.05	0.08	0.87
2-stream $f_c = 0$	0.03	0.07	0.89
2-stream $f_c = 1$	0.08	0.11	0.86

Figure 3. Average albedos for snow-covered MODIS pixels (dots) and simulations with equation (1) (solid lines), equation (2) (crosses), and the two-stream approximation (triangles) using MODIS land cover. Dashed lines show albedos simulated with equation (1) using AVHRR land cover.

Figure 4. 16-day averages of albedo from MODIS (dots), equation (1) (solid lines), equation (2) (crosses), and the two-stream approximation (triangles) averaged over (a) all land points between 40 and 70°N with valid MODIS data, and cells dominated by (b) needleleaf trees, (c) grass, and (d) shrubs in the MODIS land cover.

snow-covered and snow-free albedo model parameters have been fitted to the observations, and the IMS snow cover used in the simulations is in good large-scale agreement with MODIS observations of snow cover [*Frei et al.*, 2012], it is not surprising that equation (1) matches the albedo observations well. Equation (2) and the two-stream approximation, which give higher albedos than the fitted values when snow is held in the canopy of needleleaf forests, give

slight overestimates of winter albedo; this is more apparent in Figure 4b, which shows averages over cells with greater than 50% needleleaf tree fractions. Even so, these albedo biases are much smaller than some of those reported by *Roesch* [2006] for CMIP3 models. *Roesch and Roeckner* [2006] found winter albedos for boreal forests to be much too high in ECHAM5, which uses equation (2), but that was due to the use of unrealistically low values for plant area indices.

[15] Simulations with equation (1) match observations for needleleaf tree (Figure 4b) and grass (Figure 4c) dominated cells. For shrubs (Figure 4d), the midwinter and summer albedos are matched, but the simulation fails to reproduce an observed albedo increase in March and April; this occurs as more high-latitude shrub tundra areas with remaining snow cover become sunlit in spring and can be observed by MODIS. All of the simulations tend to give higher albedos than the observations while snow cover is expanding between October and December. *Dutra et al.* [2012] noted a similar tendency in simulations with the ECMWF model.
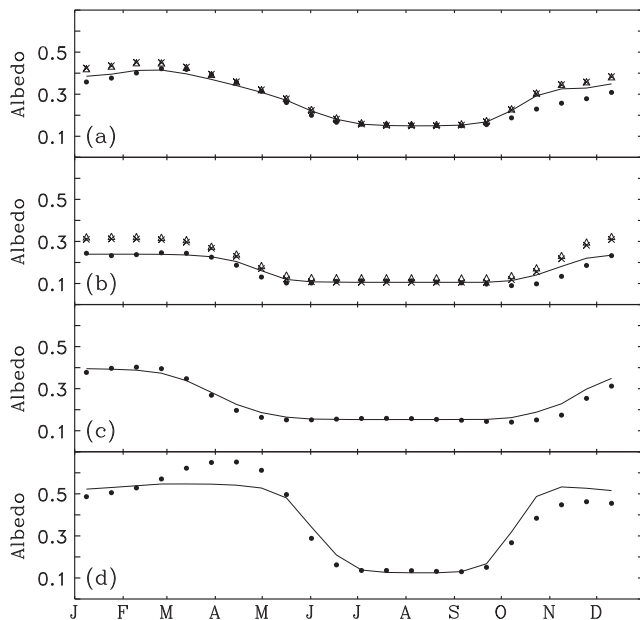
4. Conclusions

[16] Three methods commonly used in climate models for calculating the albedo of vegetated surfaces with snow cover have been compared with observations. Despite great differences in complexity, the three parametrizations gave similar predictions for spatial and temporal variations in albedo. A parametrization that was fitted to the observations naturally gave the lowest errors, but this highly accurate fitting was achieved by the adjustment of just four parameters (the albedos of needleleaf tree, broadleaf tree, grass, and shrub PFTs with snow cover). Most of the correlation between predicted and observed albedos came from land cover data. Fitting MODIS-derived land cover to MODIS albedo maps gave lower errors and higher correlation than fitting an older AVHRR-derived land cover data set that is widely used in

4

climate modeling. The fitted parameters depend on the land cover data used and should be regarded as effective values; this complicates comparisons between large-scale model parameters and small-scale field measurements [*Román et al.*, 2009].

[17] Differences in albedo have to be weighted by regional variations in incoming solar radiation to estimate impacts on surface energy balance, but as a simple measure of uncertainty, *Qu and Hall* [2013] calculated that the average albedo for snow-covered land in CMIP5 models ranged between 0.39 and 0.75. Here the range produced with existing parametrizations and land cover data in snow-covered albedo simulations was only 0.49–0.54. It is clear that some current climate models still use unrealistic vegetation parameters or distributions. Improved understanding of snow and radiation interactions with forest canopies is required, but reducing the spread of snow albedo simulations in the next generation of climate models should be straightforward with existing knowledge.

[19] The Editor thanks Ray Anderson and an anonymous reviewer for their assistance in evaluating this paper.

References

Barlage, M., X. Zeng, H. Wei, and K. E. Mitchell (2005), A global 0.05° maximum albedo dataset of snow-covered land based on MODIS observations, *Geophys. Res. Lett.*, *32*, L17405, doi:10.1029/2005GL022881.

Bartlett, P. A., M. D. MacKay, and D. L. Verseghy (2006), Modified snow algorithms in the Canadian Land Surface Scheme: Model runs and sensitivity analysis at three boreal forest stands, *Atmos. Ocean*, *44*, 207–222.

Bonan, G. B., D. Pollard, and S. L. Thompson (1992), Effects of boreal forest vegetation on global climate, *Nature*, *359*, 716–718.

Bonan, G. B., S. Levis, L. Kergoat, and K. W. Oleson (2002), Landscapes as patches of plant functional types: An integrating concept for climate and ecosystem models, *Global Biogeochem. Cycles*, *16*(2), 1021, doi:10.1029/2000GB001360.

Bonan, G. B., S. Levis, S. Sitch, M. Vertenstein, and K. W. Oleson (2003), A dynamic global vegetation model for use with climate models: Concepts and description of simulated vegetation dynamics, *Global Change Biol.*, *9*, 1543–1566, doi:10.1046/j.1529-8817.2003.00681.x.

Brovkin, V., T. Raddatz, C. H. Reick, M. Claussen, and V. Gayler (2009), Global biogeophysical interactions between forest and climate, *Geophys. Res. Lett.*, *36*, L07405, doi:10.1029/2009GL037543.

Cox, P. M., R. A. Betts, C. B. Bunton, R. L. H. Essery, P. R. Rowntree, and J. Smith (1999), The impact of new land surface physics on the GCM simulation of climate and climate sensitivity, *Clim. Dyn.*, *15*, 183–203.

Dee, D. P., et al. (2011), The ERA-Interim reanalysis: Configuration and performance of the data assimilation system, *Q. J. R. Meteorolog. Soc.*, *137*, 553–597.

Dickinson, R. E. (1983), Land surface processes and climate: Surface albedos and energy balance, *Adv. Geophys.*, *25*, 305–353.

Dutra, E., P. Viterbo, P. M. A. Miranda, and G. Balsamo (2012), Complexity of snow schemes in a climate model and its impact on surface energy and hydrology, *J. Hydrometeorol.*, *13*, 521–538, doi:10.1175/JHM-D-11-072.1.

Essery, R. L. H., M. J. Best, R. A. Betts, and P. M. Cox (2003), Explicit representation of subgrid heterogeneity in a GCM land surface scheme, *J. Hydrometeorol.*, *4*, 530–543.

Flanner, M. G., K. M. Shell, M. Barlage, D. K. Perovich, and M. A. Tschudi (2011), Radiative forcing and albedo feedback from the Northern Hemisphere cryosphere between 1979 and 2008, *Nat. Geosci.*, *4*, 151–155, doi:10.1038/NGEO1062.

Frei, A., M. Tedesco, S. Lee, J. Foster, D. K. Hall, R. Kelly, and D. A. Robinson (2012), A review of global satellite-derived snow products, *Adv. Space Res.*, *50*, 1007–1029, doi:10.1016/j.asr.2011.12.021.

Hansen, M., R. DeFries, J. R. G. Townshend, and R. Sohlberg (2000), Global land cover classification at 1km resolution using a decision tree classifier, *Int. J. Remote Sens.*, *21*, 1331–1365.

Helfrich, S. R., D. McNamara, B. H. Ramsay, T. Baldwin, and T. Kasheta (2007), Enhancements to and forthcoming developments in the Interactive Multisensor Snow and Ice Mapping System (IMS), *Hydrol. Processes*, *21*, 1576–1586.

Houldcroft, C. J., W. M. F. Grey, M. Barnsley, C. M. Taylor, S. O. Los, and P. R. J. North (2009), New vegetation albedo parameters and global fields of soil background albedo derived from MODIS for use in a climate model, *J. Hydrometeorol.*, *10*, 183–198, doi:10.1175/2008JHM1021.1.

Lawrence, P. J., and T. N. Chase (2007), Representing a new MODIS consistent land surface in the Community Land Model (CLM 3.0), *J. Geophys. Res.*, *112*, G01023, doi:10.1029/2006JG000168.

Loveland, T. R., B. C. Reed, J. F. Brown, D. O. Ohlen, Z. Zhu, L. Yang, and J. W. Merchant (2000), Development of a global land cover characteristics database and IGBP DISCover from 1 km AVHRR data, *Int. J. Remote Sens.*, *21*, 1303–1330.

Moody, E. G., M. D. King, C. B. Schaaf, D. K. Hall, and S. Platnick (2007), Northern Hemisphere five-year average (2000–2004) spectral albedos of surfaces in the presence of snow: Statistics computed from Terra MODIS land products, *Remote Sens. Environ.*, *111*, 337–345, doi:10.1016/j.rse.2007.03.026.

Oleson, K. W., et al. (2010), *Technical description of version 4.0 of the Community Land Model (CLM), NCAR Technical Note NCAR/TN-478+STR*, National Center for Atmospheric Research, Boulder, CO.

Pinty, B., N. Gobron, J.-L. Widlowski, T. Lavergne, and M. M. Verstraete (2004), Synergy between 1-D and 3-D radiation transfer models to retrieve vegetation canopy properties from remote sensing data, *J. Geophys. Res.*, *109*, D21205, doi:10.1029/2004JD005214.

Qu, X., and A. Hall (2007), What controls the strength of snow-albedo feedback?, *J. Clim.*, *20*, 3971–3981.

Qu, X., and A. Hall (2013), On the persistent spread in snow-albedo feedback, *Clim. Dyn.*, doi:10.1007/s00382-013-1774-0.

Randall, D. A., et al. (2007), Climate models and their evaluation, in *Climate Change 2007: The Physical Science Basis. Contribution of Working Group I to the Fourth Assessment Report of the Intergovernmental Panel on Climate Change*, edited by S. Solomon et al., pp. 589–662, Cambridge Univ. Press, Cambridge, U. K. and New York.

Robinson, D. A., and G. Kukla (1984), Albedo of a dissipating snow cover, *J. Clim. Appl. Meteorol.*, *23*, 1626–1634.

Robinson, D. A., and G. Kukla (1985), Maximum surface albedo of seasonally snow-covered lands in the Northern Hemisphere, *J. Clim. Appl. Meteorol.*, *24*, 402–411.

Roesch, A. (2006), Evaluation of surface albedo and snow cover in AR4 coupled climate models, *J. Geophys. Res.*, *111*, D15111, doi:10.1029/2005JD006473.

Roesch, A., and E. Roeckner (2006), Assessment of snow cover and surface albedo in the ECHAM5 general circulation model, *J. Clim.*, *19*, 3828–3843.

Román, M. O., et al. (2009), The MODIS (Collection V005) BRDF/albedo product: Assessment of spatial representativeness over forested landscapes, *Remote Sens. Environ.*, *113*, 2476–2498, doi:10.1016/j.rse.2009.07.009.

Schaaf, C. B., et al. (2002), First operational BRDF, albedo nadir reflectance products from MODIS, *Remote Sens. Environ.*, *83*, 135–148.

Thomas, G., and P. R. Rowntree (1992), The boreal forests and climate, *Q. J. R. Meteorolog. Soc.*, *118*, 469–497.

Verseghy, D., N. A. McFarlane, and M. Lazare (1993), CLASS: A Canadian Land Surface Scheme for GCMs. II Vegetation model and coupled runs, *Int. J. Climatol.*, *13*, 347–370.

Viterbo, P., and A. K. Betts (1999), Impact on ECMWF forecasts of changes to the albedo of the boreal forests in the presence of snow, *J. Geophys. Res.*, *104*, 27,803–27,810.

Widlowski, J.-L., et al. (2007), Third Radiation Transfer Model Intercomparison (RAMI) exercise: Documenting progress in canopy reflectance models, *J. Geophys. Res.*, *112*, D09111, doi:10.1029/2006JD007821.

Wilson, M. F., and A. Henderson-Sellers (1985), A global archive of land cover and soils data for use in general circulation models, *J. Climatol.*, *5*, 119–143.